Effect of noise on solid-to-liquid transition in small granular systems under shear

Martin F. Melhus,[1,2] Igor S. Aranson,[2] Dmitri Volfson,[3] and Lev S. Tsimring[3]
[1]*Department of Physics, Northwestern University, 2145 Sheridan Road, Evanston, Illinois 60208-3112, USA*
[2]*Materials Science Division, Argonne National Laboratory, 9700 South Cass Avenue, Argonne, Illinois 60439, USA*
[3]*Institute for Nonlinear Science, University of California, San Diego, La Jolla, California 92093-0402, USA*
(Received 18 May 2009; published 15 October 2009)

The effect of noise on the solid-to-liquid transition of a dense granular assembly under planar shear is studied numerically using soft-particle molecular dynamics simulations in two dimensions. We focus on small systems in a thin planar Couette cell, examining the bistable region while increasing shear, with varying amounts of random noise, and determine statistics of the shear required for fluidization. In the absence of noise, the threshold value of the shear stress depends on the preparation of the system and has a broad distribution. However, adding force fluctuations both lowers the mean threshold value of the shear stress and decreases its variability. This behavior is interpreted as thermoactivated escape through a fluctuating barrier.

DOI: 10.1103/PhysRevE.80.041305 PACS number(s): 45.70.Mg, 45.70.Qj

I. INTRODUCTION

In the last few years there have been many experimental and theoretical studies [1–17] that explored a broad range of granular flow conditions, from rapid dilute flows to slow dense flows, as well as the details of the shear-driven fluidization transition [18]; for a more recent review see [19]. While dilute granular flows can be consistently described by the kinetic theory of dissipative granular gases [20,21], dense granular flows still present significant difficulty in formulation of a continuum theory (see, e.g., [6,10,11,13,14]). Sheared dense granular assemblies undergo a bistable hysteretic transition; from a static solidlike state they experience a fluidization transition as shear increases and flow ensues. From a flowing state, while reducing shear, the granular "fluid" freezes and flow arrest occurs. For the flows under consideration, the "melting" transition occurs at a greater level of shear than the "freezing" transition. These melting-freezing transitions play a key role in understanding of the onset of effective granular friction (see, e.g., [4,6,9]) and are relevant for quantitative description of broad range of granular flows, such as avalanches and shear bands [22].

In our earlier works [11] we developed a phenomenological order parameter theory of shear-induced fluidization (partial fluidization theory). The theory was tested and validated by soft-particle molecular dynamics simulations in [12] and compared with recent experimental studies of dense granular flows on incline plane [22]. We define the order parameter ρ as a fraction of static contacts Z_s among all contacts between particles Z, $\rho=Z_s/Z$. We proposed the constitutive relation for stresses based on the splitting of the shear stress tensor into a "fluid part" proportional to the strain rate tensor and a remaining "solid part." The ratio of these two parts is a function of the order parameter. Surprisingly, the rheology of the fluid component agrees well with the kinetic theory of granular fluids even in the dense regime (see [12,22]). The partial fluidization theory was applied to a broad range of granular flows, from avalanches to stick-slip flows, and good qualitative and sometime quantitative agreement was obtained (see [11,12,22]).

The studies in Refs. [11,12,22] were performed in the situation when the granular material is energized by pure shear. However, in many experimental situations the shear is often accompanied by fluctuations either intrinsic or due to external vibrations. For example, in a recent study [17] the fluidization transition was investigated in the presence of both shear and vibration, and nontrivial interplay of the shear and vibration governing the "freezing or melting" transition was observed, including hysteretic onset of flow at nonzero amplitudes of vibrational acceleration. In addition, it was recently understood that propagation of sound waves in granular packings, which can be interpreted as microscopic vibration of grains, has a highly nontrivial effect on elastic response near the jamming transition and, in turn, influences the onset of flow [23]. Beside the anticipated decreasing of the threshold value of the shear stress (yield stress) for the onset of fluidization, noise may also have other manifestations, such as slow creeping motion even below the yield stress (compare, for example, with thermally activated motion of dislocations in crystals). Incorporation of fluctuation effects in a continuum description of dense granular flows remains a very challenging problem.

In this paper we study these phenomena numerically using soft-particle molecular dynamics simulations in a relatively small planar Couette cell. To model the effect of vibration we subject each particle to a fluctuating force at each time step. Forces acting on different particles are independent. Due to the finite system size, the fluidization transition occurred in a finite range of the applied stress values. We observe that mean value of the shear stress corresponding to the fluidization transition decreases with increasing noise level. At the same time, the width of the fluidization transition exhibits a nonmonotonic dependence on the noise level. We discuss an extension of the partial fluidization theory which allows one to take fluctuations into account when describing the shear fluidization transition. We also demonstrate that semiquantitatively the results can be interpreted as a thermoactivated escape through a fluctuating barrier.

II. MOLECULAR DYNAMICS SIMULATIONS

We consider a granular layer in a planar Couette geometry driven by a moving upper plate of mass M and length L_x.

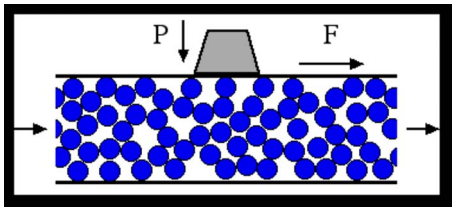

FIG. 1. (Color online) Sketch of the granular shear flow model, P is applied pressure, and F is applied shearing force, held constant over each run step. Periodic boundary conditions are applied in the flow direction (x axis).

The plate is separated from bottom by nominal distance L_y, but it is supported by the grains and is free to move vertically. We use a fixed coordinate frame with horizontal axis x, vertical axis y, and the origin at the bottom of the layer. The system is sheared by applying a constant force F to the top plate (see Fig. 1). All variables and parameters are scaled by the acceleration due to gravity g, particle size d_p, and mass m_p.

To model the interaction of individual grains we use the so-called soft-contact approach described in detail in [12,15,16]. The grains are assumed to be noncohesive, dry, inelastic disklike particles. Two grains interact via normal and shear forces whenever they overlap. For the normal impact we employ the *spring-dashpot* model [24]. This model accounts for repulsion and dissipation; the repulsive component is proportional to the degree of the overlap, and the velocity dependent damping component simulates the dissipation. The model for shear force is based on the technique developed by Cundall and Strack [25]. It incorporates tangential elasticity and the Coulomb law of friction. The elastic restoring force is proportional to the integrated tangential displacement during the contact and limited by the product of the friction coefficient and the instantaneous normal force. The grains possess two translational and one rotational degree of freedom. The motion of a grain is obtained by integrating the Newton equations by the fifth-order Gear prediction-correction method with the forces and torques produced by its interactions with all the neighboring grains and walls of the container. A noise force is added to each particle at each time step. The noise is isotropic, distributed randomly in magnitude and direction, scaled by the maximum noise force value η, and normalized to the applied pressure P (times a characteristic length of 1). These criteria produce a noise force $\vec{f}_\eta$ (with magnitude r and direction θ). Additionally, a factor of $\sqrt{dt}$ is included to correct for the effect of integrating this noise force. The resulting forces and the probability density of these forces are

$$\vec{f}_\eta(r,\theta) = \frac{P\eta}{\sqrt{dt}} r \begin{cases} r \in [0,1] \\ \theta \in [0,2\pi], \end{cases} \tag{1}$$

$$\text{prob}(\vec{f}_\eta) = \begin{cases} 0, & r > \eta \\ \dfrac{1}{(2\pi\eta)\cdot r}, & r \le \eta. \end{cases} \tag{2}$$

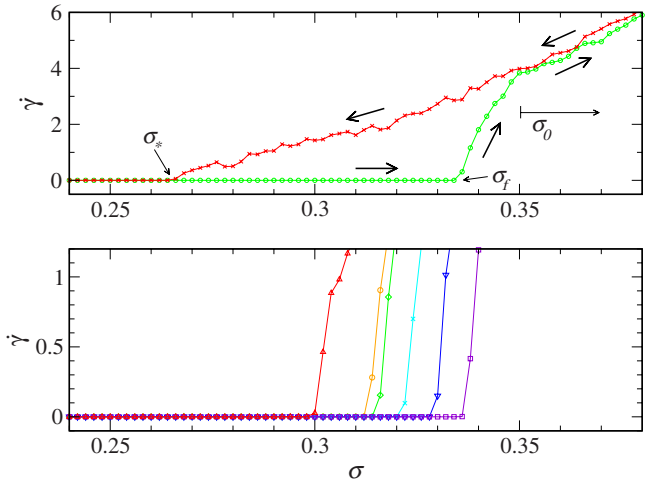

FIG. 2. (Color online) Typical dependence of shear stain rate $\dot{\gamma}=\partial v_x/\partial y$ on applied shear σ (without noise). Upper plot illustrates bistability of the onset of fluidization; arrows indicate direction of changing shear stress. Note that the value of σ_0 cannot be determined from one sample run, but it must be larger than 0.35, where the upward and downward runs separate. Lower plot shows the variability of fluidization onset from different initial configurations (note different scales in the strain rate $\dot{\gamma}$).

We used the following protocol to prepare the initial state: particles are lowered pseudorandomly into the cell, stopping when they contact another particle. After all the particles are placed, the top of the cell is lowered onto the bed, and a low level of shear is applied for the duration of a typical run. This initial state is saved and used to begin a set of runs.

Representative dependencies of the shear strain rate $\dot{\gamma}$ on applied shear stress $\sigma=F/L_x$, without noise, are shown in Fig. 2. The dependencies are obtained by ramping the shear σ by small steps $d\sigma=0.002$ from $\sigma=0.200$ to a value above the transition. At each value of σ, the system is run for 20 dimensionless time units. After the onset of flow, one can observe the hysteresis by decreasing σ well below the transition point. Note that for different initial conditions the mean transition to flow, at shear σ_m, typically occurs at different values. This variability of the transition values is obviously related to the relatively small system size (we used only 500 particles). We expect that the relative range of the transition values decreases with the number of particles. However, since in the majority of granular flows the number of particles is still not macroscopically large (compared, for example, to molecular gases), the variability of the fluidization transition remains an important issue in laboratory-scale systems, such as used in Refs. [17,22].

In order to characterize the statistical properties of the fluidization transition we studied the probability distributions $S(\sigma_f)$ of the fluidization transition values σ_f for different noise levels and initial system configurations (see Figs. 3 and 4). The individual histograms of $S(\sigma_f)$ were obtained from 100 realizations of the noise for each of different initial conditions. Figure 3 shows the histograms of $S(\sigma_f)$ obtained from averaging individual probability distribution functions (PDFs) over 20 different initial system preparations. One sees that these averaged histograms are broadly localized in

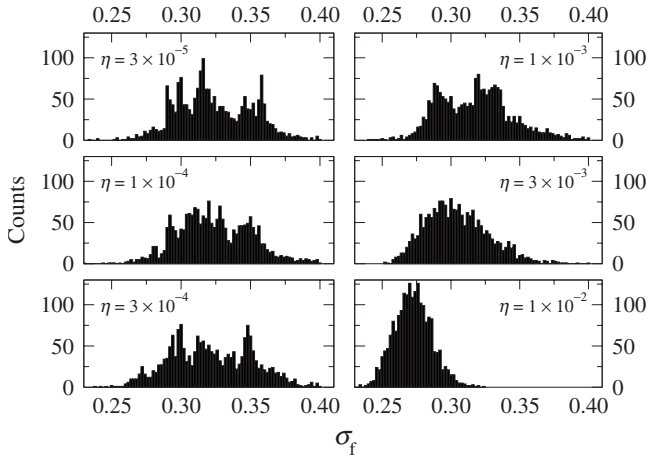

FIG. 3. Probability distributions of the fluidization transitions values σ_f for different noise levels η. All scales are identical, and each plot includes 2000 realizations from 20 different initial conditions.

some range around the mean value $\sigma_m = \int_0^{\sigma_{max}} \sigma S(\sigma) d\sigma$, and the variability of the transition value (characteristic length of this interval) is $\Delta\sigma = \sqrt{\int_0^{\sigma_{max}} (\sigma - \sigma_m)^2 S(\sigma) d\sigma}$, of the order of 10–20 % of σ_m, depending on the level of the noise. Note that at lower noise levels, changing the initial configuration produces large changes in the probability distribution compared to the variability within a given probability distribution. As a result, the probability distributions at low noise levels appear to be of comparable breadth to those at higher noise levels (compare $\eta = 3\times10^{-5}$ with $\eta = 1\times10^{-3}$), but the probability distribution from any one individual initial configuration is substantially narrower than the probability distribution from the same initial configuration at higher noise levels. This distinction is clear when contrasting Figs. 3 and 4. In Fig. 4, each initial configuration was normalized around its mean, and then all configurations were summed. The probability distributions for the runs with lower noise levels

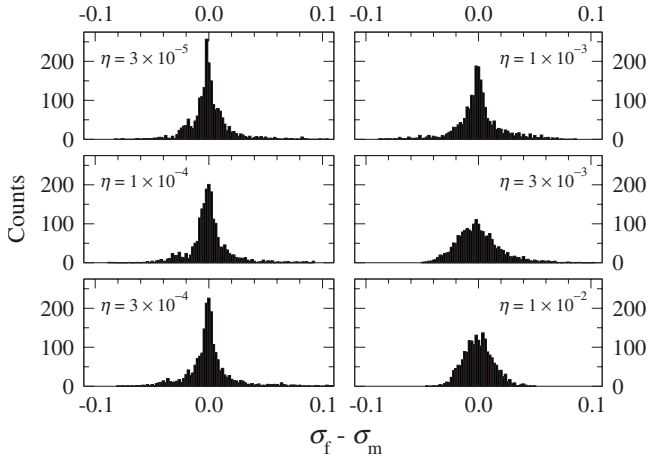

FIG. 4. Probability distributions of the fluidization transitions values σ_f for different noise levels η normalized around the mean σ_m for each individual initial configuration. All scales are identical, and each plot includes 2000 realizations from 20 different initial conditions.

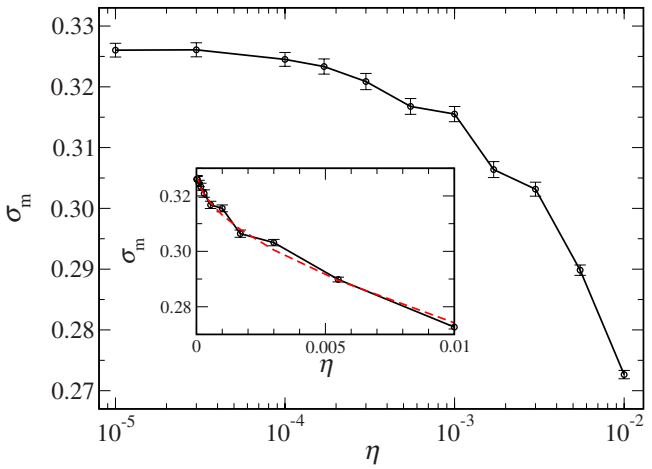

FIG. 5. (Color online) Mean fluidization shear σ_m vs noise magnitude η in semilogarithmic scale. Error bars are set at two standard deviations. Inset: σ_m vs η in linear scale. Dashed line shows fit $\sigma_m = 0.33\sqrt{1 - 0.3\,\eta^{1/2}}$.

($\eta = 3\times10^{-5}$ to $\eta = 1\times10^{-3}$) show marked narrowing as opposed to the non-normalized distributions in Fig. 3. Further, the individual initial configurations showed increasing, decreasing, or approximately constant values of σ_f with increasing noise η; only averaging over several initial configurations gives a proper statistical understanding of how these variables change with increasing noise.

The dependence of σ_m versus the noise level is shown in Fig. 5 (error bars at two standard deviations). We observe a monotonic decrease of the transition value σ_m as the noise strength increases; however effect is relatively mild even for large noise strengths. Due to the finite time of integration for small values of the shearing force F, small noise levels η, and time averaging the measurements of the top plate velocity, we did not observe slow creep. By the analogy with the thermoactivated motion we anticipate that the creep velocity V should be of the order $V \sim \exp[-\text{const} \times \eta/F] \ll 1$. We did, however, observe occasional microrearrangement events into another, presumably more stable, configuration, indicated by a short period of creep followed by another long period of flow arrest. We distinguish these microrearrangement events from true fluidization. The effect of microrearrangements on the packing fraction is readily visible (see Fig. 6). Each of the selected runs has small microrearrangement events as the shear increases, visible as a small decrease in the packing fraction followed by a period where the packing fraction remains constant. And while these microrearrangement events are accompanied by a short increase in top plate velocity, the top plate velocity rapidly returns to zero unlike when true fluidization occurs. As such, these velocity transients would not be readily observable on a graph such as the upper plot of Fig. 2.

Figure 7 illustrates noise dependence of the width of the fluidization transition calculated by two different types of averaging. If the averaging is performed simultaneously over all initial conditions and noise realizations, the fluidization transition width $\Delta\sigma$ decreases fairly monotonously with the noise strength. We call the widths calculated by this method the absolute widths. In contrast, if the width of the fluidiza-

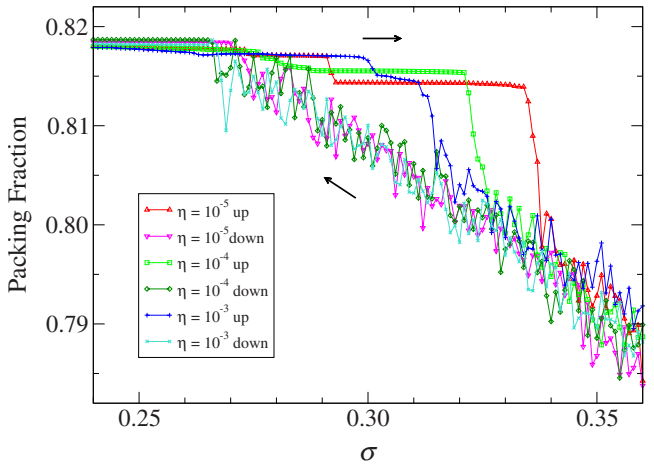

FIG. 6. (Color online) Packing fraction for selected runs as a function of applied shear at different noise levels. Arrows indicate direction of changing shear. In contrast, for example, with Fig. 2 in Ref. [17], noting that random close packing fraction is higher in two dimensions.

tion transition distribution is first computed over noise realizations for the same initial condition and *then* averaged over initial conditions, this quantity, $\Delta\bar{\sigma}$, exhibits nonmonotonic behavior, first increasing at small noise $\eta < 0.002$ and then decreasing at larger η [26]. We call these widths conditional widths. Comparing distributions in Figs. 3 and 4 we see that the difference in these two measures reflects the nature of the noise-driven fluidization. For a fixed initial configuration, at small noise the distribution of the fluidization thresholds is narrow, as it should be expected, and it widens with increasing the noise level. However, at large noise level, the distribution "collapses" near a critical value of shear stress $\sigma_* \approx 0.25$ and the distribution width is decreasing there. On the other hand, different initial configurations lead to different critical fluidization stresses σ_0 within a certain range (see Fig. 2); averaging over different initial conditions leads to a large spread of the transition width even at smaller noise levels. As the stress increases to the stress value σ_*, the different distributions, calculated from different initial configurations, exhibit an overall monotonic decrease in width. Note that variability of the critical shear stress σ_0 is presumably a consequence of a small system size in our numerical experiments. In large systems, this variability should decrease.

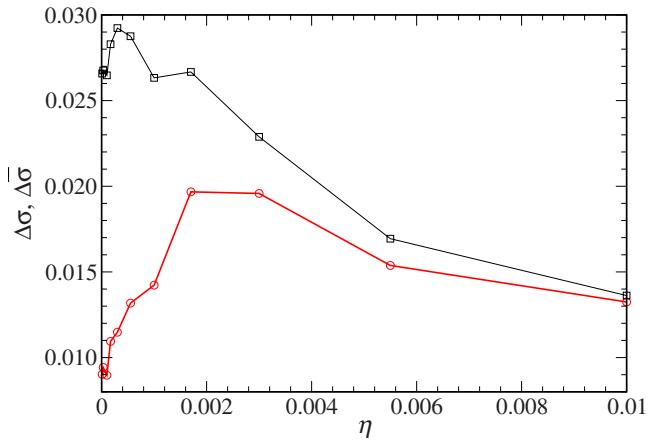

FIG. 7. (Color online) The widths of the transition range. Absolute width $\Delta\sigma$ (squares, upper curve) and conditional width $\Delta\bar{\sigma}$ (circles, lower curve) vs noise magnitude η.

III. EXTENSION OF PARTIAL FLUIDIZATION THEORY

In the partial fluidization theory the order parameter ρ is governed by the Ginzburg-Landau-type equation for the first-order phase transition [11,12,22],

$$\partial_t + \mathbf{v}\,\nabla\,\rho = D\nabla^2\rho + (1-\rho)f(\rho,\delta_s), \tag{3}$$

where $\mathbf{v}$ is the velocity field, D is the diffusion coefficient controlling, for example, the width of the granular solid or liquid interface, and f is a certain nonlinear function of the order parameter which can be extracted from molecular dynamics simulations [12,22]. In the absence of external vibrations, the control parameter δ_s or shear temperature is a function of the ratio of shear stress σ_s to normal stress σ_n, $\delta_s \sim \Phi(\sigma_s/\sigma_n)$. The fluidization occurs when the "shear temperature" δ_s exceeds a certain critical value δ_* (compare to Mohr-Coulomb failure criterion). From the symmetry arguments (i.e., the value of δ_s should not depend on the sign of shear stress), a simple expression for the control parameter δ_s was proposed in our previous work,

$$\delta_s = \frac{(\sigma_s/\sigma_n)^2 - \phi_1^2}{\phi_2^2 - \phi_1^2}, \tag{4}$$

where ϕ_1 and ϕ_2 are tangents of corresponding dynamic and static repose angles.

In the presence of random fluctuations one may anticipate that the contributions from the shear and from the noise will be additive at least for moderate values of the noise strength η. Therefore, a plausible generalization of Eq. (4) is the following:

$$\delta_s = \frac{(\sigma_s/\sigma_n)^2 - \phi_1^2}{\phi_2^2 - \phi_1^2} + \chi(\eta), \tag{5}$$

where χ is some function of the noise strength η. This additive contribution of noise may explain the observed reduction of the mean value of the shear stress needed for fluidization in the presence of noise. The function χ can be evaluated from comparison with molecular dynamics simulations shown in Fig. 5. Since the transition to fluidization occurs for $\delta_s = \delta_* = \text{const}$, for the typical value of shear stress at the transition $\sigma_s = \sigma_*$ we obtain from Eq. (5) (since $F_m = \sigma_s/L_x$)

$$F_m = \alpha_2\sqrt{1-\beta_2\chi(\eta)}, \tag{6}$$

where α_2, β_2 are constants. The data presented in the inset of Fig. 5 can be fitted by Eq. (6) with $\chi(\eta) = \sqrt{\eta}$, $\alpha_2 = 0.33$, and $\beta_2 = 0.3$.

IV. INTERPRETATION IN TERMS OF THERMOACTIVATED ESCAPE THEORY

The generalization of the partial fluidization theory described in Sec. III may explain the reduction of the shear

stress needed for fluidization, but as a deterministic theory it is unable to explain the nontrivial observed behavior of the distribution of fluidization thresholds for different noise realizations and initial configurations of grains. However, one can formulate a semiquantitative stochastic model of the fluidization transition by combining the partial fluidization theory with the ideas of a thermoactivated transition in a bistable system [27]. According to the partial fluidization model, in the range of shear stresses $\sigma_* < \sigma < \sigma_0$ the granular layer is in a bistable regime where both static and flowing states are viable. In the presence of noise fluctuations these two stable states become metastable, and a spontaneous transition from one regime to the other is possible. The rate of this transition, of course, depends on the applied shear stress and the noise magnitude. Therefore, we postulate that setting the plate into motion is equivalent to a noise-driven escape process from a metastable static regime to a metastable flowing regime through a potential barrier. Increasing the shear stress effectively decreases the barrier until it becomes so small that the plate escapes with high probability within a certain "waiting time" t_0 for each value of stress. In our numerical experiments time t_0 is the time the system is kept at a fixed value of the shear stress before it is ramped up to the next fixed value.

If the potential barrier is $\Delta\Pi$, the distribution of escape times for applied stress σ is exponential $f(t|\sigma,\sigma_b) = t_m^{-1} \exp(-t/t_m)$ with the mean escape time $t_m \sim \exp[\Delta\Pi/T]$, where T is the noise temperature. The height of the potential barrier depends on the applied shear stress σ in a nontrivial way. It is zero if the shear stress is greater than static fluidization threshold σ_0 and it is effectively infinite if $\sigma < \sigma_*$, where σ_* is the minimal shear stress supporting flowing regime (see Fig. 2). It reflects the fact that for $\sigma < \sigma_*$, the flowing regime does not exist (we do not consider here extremely high values of noise at which the entire granular layer becomes fluidized even in the absence of shear stress). Thus, we model this dependency by assuming

$$\Delta\Pi = \frac{\sigma_0 - \sigma}{\sigma - \sigma_*} \tag{7}$$

so

$$f(t|\sigma,\sigma_b) = \exp\left[\frac{\sigma - \sigma_0}{(\sigma - \sigma_*)T}\right] \exp\left\{-t \exp\left[\frac{\sigma - \sigma_0}{(\sigma - \sigma_*)T}\right]\right\}. \tag{8}$$

The probability that the plate begins to move within certain time t_0 is given by

$$p(\sigma|\sigma_0) = \int_0^{t_0} f(t|\sigma)dt = 1 - \exp\{-t_0 \exp[(\sigma - \sigma_0)/T(\sigma - \sigma_*)]\} \tag{9}$$

and it goes up from zero at $\sigma = \sigma_*$ to 1 at $\sigma \to \infty$. The probability distribution of the "critical slipping stresses" is given by

$$F(\sigma|\sigma_0) = dp(\sigma)/d\sigma = \frac{t_0(\sigma_0 - \sigma_*)}{T(\sigma - \sigma_*)^2} f(t_0|\sigma,\sigma_0). \tag{10}$$

As we have shown above, the shear stress needed for fluidization depends on the initial arrangement of grains, so σ_0 varies within a certain range $(\sigma_{min}, \sigma_{max})$ (note however that the value of σ_* is independent of initial conditions since flowing regime is presumably ergodic). So, formula (9) should be generalized,

$$F_1(\sigma) = \int_{\sigma_{min}}^{\sigma_{max}} P(\sigma_0) F(\sigma|\sigma_0) d\sigma_0 = \frac{t_0}{T(\sigma - \sigma_*)^2} \int_{\sigma_{min}}^{\sigma_{max}} (\sigma_0 - \sigma_*) P(\sigma_0) f(t_0|\sigma,\sigma_0) d\sigma_0. \tag{11}$$

From this formula one can find the mean and width of F_1 as a function of temperature.

We introduce two types of widths for the fluidization transition width, $\Delta\sigma$. The first or conditional width, $\Delta\bar{\sigma} = (\langle \bar{\sigma}_2 - \bar{\sigma}_1^2 \rangle)^{1/2}$, is defined as follows. First, we calculate the first and the second moments of the distribution function for *fixed* value of σ_0 and then average over the ensemble. Thus, using the distribution function equation [Eq. (10)],

$$\bar{\sigma}_1 = \int_{-\infty}^{\infty} \sigma F(\sigma|\sigma_0) d\sigma,$$

$$\bar{\sigma}_2 = \int_{-\infty}^{\infty} \sigma^2 F(\sigma|\sigma_0) d\sigma. \tag{12}$$

Then, the square of the conditional width is defined as follows:

$$\Delta\bar{\sigma}^2 = (\sigma_{max} - \sigma_{min})^{-1} \int_{\sigma_{min}}^{\sigma_{max}} (\bar{\sigma}_2 - \bar{\sigma}_1^2) d\sigma_0. \tag{13}$$

Here we assume for simplicity that the probability of barrier distribution is uniform, $P(\sigma_0) = 1/(\sigma_{max} - \sigma_{min})$.

The second (absolute) width is averaged over different initial configurations (as characterized by σ_0) and the noise realizations simultaneously,

$$\sigma_1 = (\sigma_{max} - \sigma_{min})^{-1} \int_{-\infty}^{\infty} \int_{\sigma_{min}}^{\sigma_{max}} \sigma F(\sigma|\sigma_0) d\sigma d\sigma_0,$$

$$\sigma_2 = (\sigma_{max} - \sigma_{min})^{-1} \int_{-\infty}^{\infty} \int_{\sigma_{min}}^{\sigma_{max}} \sigma^2 F(\sigma|\sigma_0) d\sigma d\sigma_0 \tag{14}$$

and the square of the absolute width

$$\Delta\sigma^2 = \sigma_2 - \sigma_1^2. \tag{15}$$

In general, $\Delta\sigma \geq \Delta\bar{\sigma}$.

Numerical evaluation of Eqs. (13) and (14) indeed shows that the noise dependencies of the mean and both widths of the fluidization transition are consistent with the molecular dynamics simulations (compare Figs. 7 and 8): the mean σ_m and the total width $\Delta\sigma$ monotonously decrease with the tem-

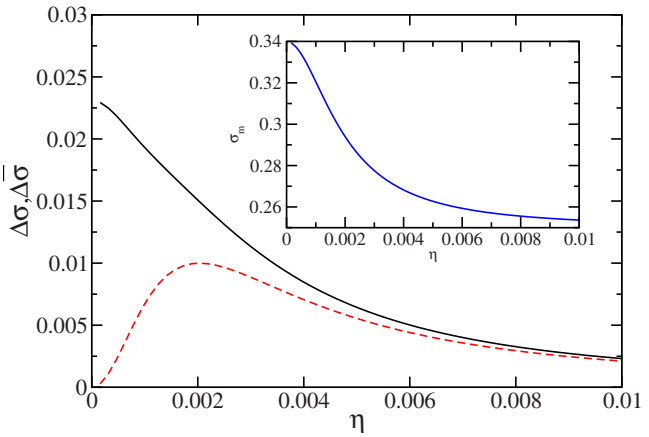

FIG. 8. (Color online) The two widths of the fluidization transition range obtained from the thermoactivated escape model [Eqs. (13) and (15)]: absolute width $\Delta\sigma$ (solid line) and conditional width $\Delta\bar{\sigma}$ (dashed line) vs noise magnitude η. Inset shows the mean value of the fluidization stress σ_m as a function of η. We use $\sigma_*=0.25$, $\sigma_{min}=0.30$, $\sigma_{max}=0.38$, $t_0=10$, and $T=10^5\eta^2$.

perature, while the conditional width, $\Delta\bar{\sigma}$, initially increases with T and then decreases. Clearly, the thermal escape model described here gives only a semiquantitative picture of the noise-activated fluidization transition. Furthermore, one cannot exclude that noise affects fluidization transition through other mechanisms. For example, it is known that vibration leads to slow compaction [1] which in turn will alter the particle configuration, which should affect the fluidization threshold. Therefore, vibration at small shear stress levels may gradually modify the range of stresses $\{\sigma_{min}, \sigma_{max}\}$, so the latter itself would be a function of the noise temperature. More in-depth theoretical analysis of the interplay between shear fluidization and fluctuation-driven compaction is needed.

In conclusion, we performed numerical studies of the effect of noise on the fluidization transition in small systems. Our results revealed a twofold effect of the noise on the fluidization transition. First, the noise decreases the mean value of the fluidization threshold. Second, noise changes the width of the distribution of critical fluidization stresses in a nontrivial way. Our simulations show that depending on averaging method, the width of the range of fluidization transition values may show qualitatively different behavior. Conditional averaging over noise fluctuations for fixed initial configurations demonstrates initial spread and eventual collapse of the distribution with the level of noise. In contrast, absolute averaging over both noise realizations and initial configurations showed a monotonic decrease of the distribution width. However, this difference in behavior may be a property of small granular assemblies only; in large systems the dependence on initial configuration presumably should disappear. Thus, we expect that in large systems, the fluidization distribution would follow the nonmonotonic behavior of the conditional width $\Delta\bar{\sigma}$. This is an interesting prediction deserving experimental verification. Our simulations also indicate a possibility to extend partial fluidization theory to the situation of simultaneous action of mechanical shear and random fluctuations. An interesting question in this context is the relation between noise and periodic mechanical vibration of the entire cell. We reserve this intriguing issue for further investigations.

ACKNOWLEDGMENTS

This research was supported by U.S. Department of Energy, Grants No. DE-AC02-06CH11357 (M.F.M. and I.S.A.) and No. DE-FG03-95ER14516 (D.V. and L.S.T.).

[1] H. Jaeger, S. Nagel, and R. P. Behringer, Rev. Mod. Phys. **68**, 1259 (1996).
[2] J. C. Tsai, G. A. Voth, and J. P. Gollub, Phys. Rev. Lett. **91**, 064301 (2003); J. C. Tsai and J. P. Gollub, Phys. Rev. E **72**, 051304 (2005).
[3] S. Siavoshi, A. V. Orpe, and A. Kudrolli, Phys. Rev. E **73**, 010301(R) (2006).
[4] GDR MiDi (collective work), Eur. Phys. J. E **14**, 341 (2004).
[5] O. Pouliquen, Phys. Fluids **11**, 542 (1999).
[6] P. Jop, Y. Forterre, and O. Pouliquen, Nature (London) **441**, 727 (2006).
[7] R. Delannay, M. Louge, P. Richard, N. Taberlet, and A. Valance, Nature Mater. **6**, 99 (2007).
[8] T. Börzsönyi and R. E. Ecke, Phys. Rev. E **76**, 031301 (2007).
[9] S. Deboeuf, E. Lajeunesse, O. Dauchot, and B. Andreotti, Phys. Rev. Lett. **97**, 158303 (2006).
[10] F. da Cruz, S. Emam, M. Prochnow, J.-N. Roux, and F. Chevoir, Phys. Rev. E **72**, 021309 (2005).
[11] I. S. Aranson and L. S. Tsimring, Phys. Rev. E **64**, 020301(R) (2001); **65**, 061303 (2002).
[12] D. Volfson, L. S. Tsimring, and I. S. Aranson, Phys. Rev. Lett. **90**, 254301 (2003); Phys. Rev. E **68**, 021301 (2003); **69**, 031302 (2004).
[13] A. Lemaitre, Phys. Rev. Lett. **89**, 064303 (2002); **89**, 195503 (2002).
[14] K. Kamrin and M. Z. Bazant, Phys. Rev. E **75**, 041301 (2007).
[15] D. Ertas *et al.*, Europhys. Lett. **56**, 214 (2001); L. E. Silbert, D. Ertas, G. S. Grest, T. C. Halsey, D. Levine, and S. J. Plimpton, Phys. Rev. E **64**, 051302 (2001).
[16] L. E. Silbert, Phys. Rev. Lett. **94**, 098002 (2005).
[17] K. E. Daniels and R. P. Behringer, Phys. Rev. Lett. **94**, 168001 (2005).
[18] We define the "fluidization transition" as the solid-to-liquid transition of the granular system. This definition keeps the nomenclature of this work consistent with reports of our previous studies.
[19] I. S. Aranson and L. S. Tsimring, Rev. Mod. Phys. **78**, 641 (2006).
[20] J. T. Jenkins and M. W. Richman, Phys. Fluids **28**, 3485 (1985).
[21] N. V. Brilliantov and Th. Pöschel, *Kinetic Theory of Granular Gases* (Oxford University Press, New York, 2004).

[22] I. S. Aranson, L. S. Tsimring, F. Malloggi, and E. Clément, Phys. Rev. E **78**, 031303 (2008).
[23] L. Bonneau, B. Andreotti, and E. Clément, Phys. Rev. Lett. **101**, 118001 (2008).
[24] J. Shäfer, S. Dippel, and D. E. Wolf, J. Phys. I **6**, 5 (1996).
[25] P. A. Cundall and O. D. L. Strack, Geotechnique **29**, 47 (1979).
[26] Figure 7 shows nonzero distribution width $\Delta\bar{\sigma}$ for very small noise magnitude η. This behavior can only be explained by amplification of round-off errors near the threshold of fluidization intensity.
[27] N. G. van Kampen, *Stochastic Processes in Physics and Chemistry*, 3rd ed. (Elsevier, New York, 2007).